Disentangling temporal and population variability in plant root water uptake from stable isotopic analysis: when rooting depth matters in labeling studies

Valentin Couvreur[1]*, Youri Rothfuss[2]*, Félicien Meunier[3], Thierry Bariac[4], Philippe Biron[4], Jean-Louis Durand[5], Patricia Richard[4], and Mathieu Javaux[1,2]

[1]Earth and Life Institute (ELI), Université catholique de Louvain (UCL), Louvain-la-Neuve, 1348, Belgium
[2]Institute of Bio- and Geosciences, IBG-3 Agrosphere, Forschungszentrum Jülich GmbH, Jülich, 52425, Germany
[3]CAVElab - Computational and Applied Vegetation Ecology, Faculty of Bioscience Engineering, Ghent University, Campus Coupure links 653, Gent, 9000, Belgium
[4]Institute of Ecology and Environmental Sciences (IEES) – Paris, UMR 7618, CNRS-Sorbonne Université, Campus AgroParisTech, Thiverval-Grignon, 78850, France
[5]UR P3F (INRA), Lusignan, 86600, France

Correspondence to: Valentin Couvreur (valentin.couvreur@uclouvain.be) and Youri Rothfuss (y.rothfuss@fz-juelich.de)

* These authors contributed equally to this work.

Abstract. Isotopic labeling techniques have the potential to minimize the uncertainty of plant root water uptake (RWU) profiles estimated through multi-source (statistical) modeling, by artificially enhancing soil water isotopic gradient. On the other end of the modelling continuum, physical models can account for hydrodynamic constraints to RWU if simultaneous soil and plant water status data is available.

In this study, a population of tall fescue (*Festuca arundinacae* cv Soni) was grown in a macro-rhizotron and monitored for a 34-hours long period following the oxygen stable isotopic (^{18}O) labeling of deep soil water. Aboveground variables included tiller and leaf water oxygen isotopic compositions (δ_{tiller} and δ_{leaf}) as well as leaf water potential (ψ_{leaf}), relative humidity, and transpiration rate. Belowground profiles of root length density (RLD), soil water content and isotopic composition were also sampled. While there were strong correlations between hydraulic variables as well as between isotopic variables, the experimental results underlined the partial disconnection between temporal dynamics of hydraulic and isotopic variables.

In order to dissect the problem, we reproduced both types of observations with a one-dimensional physical model of water flow in the soil-plant domain, for 60 different realistic RLD profiles. While simulated ψ_{leaf} followed clear temporal variations with little differences across plants as if they were "on board of the same rollercoaster", simulated

δ_{tiller} values within the plant population were rather heterogeneous ("swarm-like") with relatively little temporal variation and a strong sensitivity to rooting depth. The physical model thus explained the discrepancy between isotopic and hydraulic observations: the variability captured by δ_{tiller} reflected the spatial heterogeneity in rooting depth in the soil region influenced by the labeling and may not correlate with the temporal dynamics of ψ_{leaf}. In other words, the strong variations of RWU as deduced from isotopic changes in the tiller water may not translate into significant variations of leaf water potential value.

For comparison purposes, a Bayesian statistical model was also used to simulate RWU. While they predicted relatively similar cumulative RWU profiles, the physical model could differentiate spatial from temporal dynamics of the isotopic composition. An important difference between the two types of RWU models was the ability of the physical model to simulate the occurrence of hydraulic lift in order to explain concomitant increases of soil water content and isotopic composition observed overnight above the soil labeling region.

List of variables with symbols and units

Name	Symbol	Units
Leaf water potential/head:	ψ_{leaf}	MPa
Soil water potential/head:	ψ_{soil}	MPa
Water volumetric mass:	ρ_w	kg m^{-3}
Soil apparent density:	ρ_b	kg m^{-3}
Soil gravimetric water content:	θ_{grav}	kg kg^{-1}
Soil volumetric water content:	θ	m^3 m^{-3}
Intensity of water uptake (sink term):	S	d^{-1}
Transpiration rate per unit soil area:	T	m d^{-1}
Air relative humidity	RH	%
Soil horizontal area:	A_{soil}	m^2
Soil layer depth (for each layer):	z	m
Soil layer thickness (for each layer):	ΔZ	m
Root length (for each soil layer):	l_{root}	m
Relative Root Water Uptake	rRWU	dimensionless
Best run	br	dimensionless
Root Length Density:	RLD	m m^{-3}
Soil water oxygen isotopic composition:	δ_{soil}	‰
Tiller water oxygen isotopic composition:	δ_{tiller}	‰
Leaf water oxygen isotopic composition:	δ_{leaf}	‰
Soil-root system conductance:	$K_{soil\text{-}root}$	m^3 MPa^{-1} s^{-1}
Soil-root radial conductance:	K_{radial}	m^3 MPa^{-1} s^{-1}
Root radial conductivity:	L_{pr}	m MPa^{-1} s^{-1}
Root axial conductance:	K_{axial}	m^3 MPa^{-1} s^{-1}
Equivalent root axial conductivity:	k_{axial}	m^4 MPa^{-1} s^{-1}
Soil hydraulic conductivity:	k_{soil}	m^2 MPa^{-1} s^{-1}
Saturated soil hydraulic conductivity:	k_{sat}	m^2 MPa^{-1} s^{-1}
Soil hydraulic conductivity parameter	λ	dimensionless

Soil relative water content	$S_{e,j}$	dimensionless

1 Introduction

Since the seminal work of Washburn and Smith [1934] where it was first reported that willow trees did not fractionate hydrogen stable isotopes in a hydroponic water solution during root water uptake (RWU), water stable isotopologues ($^{1}H^{2}H^{16}O$ and $^{1}H_{2}{}^{18}O$) have been used as indicators for plant water sources in soils. In their review, Rothfuss and Javaux [2017] reported in the period 2015-2016 about no less than 40 publications in which RWU was retrieved from stable isotopic measurements. Novel measuring techniques (e.g., cavity ring-down spectroscopy – CRDS and off-axis integrated cavity output spectroscopy – ICOS) providing ways for fast and cost-effective water stable isotopic analyses certainly enable and emulate current research in that field. Water stable isotopologues are no longer powerful tracers waiting for technological developments [Yakir and Sternberg, 2000] but are on the verge to be used to their full potential for addressing eco-hydrological research questions and identify processes in the soil-plant-atmosphere continuum [Werner et al., 2012; Dubbert and Werner, 2019; Sprenger et al., 2016].

The isotopic determination of RWU profiles is based on the principle that the isotopic composition of xylem water at the outlet of the root system (i.e., in the first aerial and non-transpiring node of the plant) equals the sum of the product between the soil water isotopic composition and relative contribution to RWU across plant water sources. Results come only with reasonable precision when (i) the soil water isotopic composition depth gradient is strong and monotonic (thus avoiding issues of identifiability) and (ii) the temporal dynamics of RWU and soil water isotopic composition is relatively low. Condition (i) is fulfilled mostly at the surface of the soil, while soil water isotopic composition gradients become usually lower or null with increasing depth (due to the isotopic influence of the groundwater table and increasing dispersion with depth). As illustrated by Oerter and Bowen [2019], the lateral variability of the soil water isotopic composition profiles can become significant in the field and could have great implications on the representability and meaningfulness of isotopic-derived estimate of RWU profiles. Condition (ii) is often neglected but is required due to the instantaneous nature of the sap flow samples.

To overcome these limitations, labeling pulses have been increasingly used in recent works to artificially alter the natural isotopic gradients [e.g., Beyer et al., 2016; Beyer et al., 2018; Grossiord et al., 2014; Jesch et al., 2018; Volkmann et al., 2016b]. However, a precise characterization of the artificial spatial (i.e., lateral and vertical) and temporal distributions of the soil water isotopic composition (driven by e.g., soil isotopic water flow) is crucial. The punctual assessments of the isotopic composition profiles following destructive sampling in the field and subsequent extraction of water in the laboratory might neither be spatially nor temporally representative and can lead to erroneous estimates of RWU profiles [Orlowski et al., 2018; Orlowski et al., 2016a].

The vast majority of isotopic studies use statistical (e.g., Bayesian) modeling to retrieve RWU profile solely from the isotopic composition of water extracted in the soil and the shoot [Rothfuss and Javaux, 2017]. However, when data on soil and plant water status is available, hydraulic modeling tools can also be used to connect different data types in a process-based manner and estimate root water uptake profiles [Passot et al., 2019]. Some of the most simplistic models

use 1-D relative root distribution and plant-scale hydraulic parameters [Sulis et al., 2019], while the most complex rely on root architectures and root segment permeabilities [Meunier et al., 2017c]. Only a handful of studies coupled isotopic measurements in plant tissues and soil material with models describing RWU in a mechanistic manner. For instance, Meunier et al. [2017a] could both locate and quantify the volume of redistributed water by *Lolium multiflorum* by labeling of the soil with ^{18}O enriched water under controlled conditions.

Building on the work of Meunier et al. [2017a], the objective of the present study is to (i) model in a physically-based manner (i.e., by accounting for soil and plant and environmental factors) the temporal dynamics of the isotopic composition of RWU of a population of *Festuca arundinacae* cv Soni. (tall fescue) during a semi-controlled experiment following an isotopic labeling of deep soil water, (ii) investigate the implication of the model-to-data fit quality in terms of meaningfulness of the isotopic information to reconstruct RWU profiles, and finally (iii) confront the simulated root water uptake profiles with estimations obtained on basis of isotopic information alone (i.e., provided by a Bayesian mixing model).

2 Material and methods

Our experiment consisted in supplying labeled water from the bottom to a macro-rhizotron in which tall fescue was grown. Data on soil and plant oxygen stable isotopic composition and hydraulic status were monitored for 34 hours. In the following, the oxygen isotopic composition of water will be expressed in per mil (‰) on the "delta" ($\delta^{18}O$) scale with respect to the international water standard V-SMOW [Gonfiantini, 1978].

2.1 Rhizotron experimental setup

The macro-rhizotron (dimensions: 1.6 m x 1.0 m x 0.2 m, see picture in Appendix A) was placed inside a glasshouse (INRA Lusignan, France), where it was continuously weighed (KE1500, Mettler-Toledo, resolution: 20 g) to monitor water effluxes (i.e., bare soil evaporation or evapotranspiration). Underneath the soil compartment and in contact with it, a water reservoir (height: 0.1 m) filled with gravel acted as water table and allowed the supply of water to the rhizotron. The rhizotron was equipped with two sets of CS616 time domain reflectometer (TDR) profiles (Campbell Scientific, USA) with 30 cm long probe rods positioned at six depths (–0.05, –0.10, –0.30, –0.60, – 1.05 and –1.30 m) and one profile of tensiometers (SMS 2000, SDEC-France) located at four depths (–0.05, –0.10, –0.30, and –0.60 m) in order to monitor the evolution of soil water volumetric content (θ, in $m^3\ m^{-3}$) and matric potential (ψ_{soil}, in MPa). Finally, relative humidity (RH, %) was recorded above the vegetation with one humidity and temperature probe (HMP45D, Vaisala, Finland). The transparent polycarbonate sides (front and back) allowed the daily observations of root maximal depth. The experimental setup allowed precisely controlling the amount and $\delta^{18}O$ of soil input water.

Another important feature was the soil depth (i.e., 1.60 m) which minimized the influence of the water table on superficial layers water content and $\delta^{18}O$.

2.2 Soil properties and installation

The soil substrate originates from the Lp horizon of an agricultural field part of the Observatory of Environment Research (ORE), INRA Lusignan, France (0°60W, 46°250N) which is classified as District Cambisol (particle size distribution: sand 15%, silt 65%, clay 20%). Prior installation in the rhizotron, the substrate was sieved at 2 mm and dried out in an air oven at 110 °C during 48 h to remove most of the residual water. 450 kg of soil was filled in the rhizotron by 0.10 m increment and compacted in order to reach a dry bulk density value of ρ_b = 1420 kg m^{-3}. The closed-form soil water retention curve of van Genuchten [1980] was derived in a previous study by Meunier et al. [2017a] from synchronous measurements of soil water content and matric potential from saturated to residual water content (see Appendix B for its hydraulic parameters). It was used to compute the soil water matric potential (ψ_{soil}, in MPa) on basis of volumetric water content data during the present experiment.

2.3 Experimental protocol

After installation, the soil was gradually flooded with local water ($\delta^{18}O$ = –6.8 ‰) from the bottom reservoir up to the top of the profile for a period of three days in order to reduce as much as possible the initial lateral and vertical heterogeneities in water content and $\delta^{18}O$. The tall fescue (*Festuca arundinaceae* cv Soni) was sown at a seeding density of 3.6 g m^{-2} (which corresponds for the rhizotron surface area of 0.2 m^2 to roughly 300 plants) when soil water content reached 0.25 m^3 m^{-3} (corresponding to pF 2.3) at –0.05 m, as measured by the soil water sensors, and emerged 12 days later. During a period of 165 day following seeding, the tall fescue cover was exclusively watered from the reservoir with local water in order to (i) keep the soil bottom layer (< –1.3 m) close to water saturation, and to (ii) not to disrupt the natural soil water $\delta^{18}O$ profile.

166 days after seeding (DaS 166) the following conditions were fulfilled: (i) there was a strong soil water content gradient between the soil deep [–1.5 m, –1.0 m] and superficial [–0.3 m, 0 m] layers, (ii) the tall fescue roots had reached a depth of –1.5 m (observed through polycarbonate transparent sides). That same day at 17:00, the reservoir's water was labelled and its $\delta^{18}O$ measured at +470 ‰. Soil was sampled before (DaS 166 - 15:45) and after labeling on DaS 167 - 07:00, DaS 167 - 17:00 and DaS 168 - 05:00 using a 2 cm diameter auger through the transparent polycarbonate side of the rhizotron on four occasions from the surface down to –1.3 m for the determination of soil gravimetric water content (θ_{grav}, in kg kg^{-1}) and oxygen stable isotopic composition (δ_{soil}, in ‰). Gravimetric water content was then converted to volumetric water content ($\theta = \theta_{grav} * \rho_b/\rho_w$, in m^3 m^{-3}, where ρ_b is the bulk soil density and ρ_w is the water density). The hypothesis of a constant value for ρ_b across the reconstructed soil profile was further

validated from the quality of the linear fit (coefficient of determination $R^2 = 1.0$) between the θ values measured by the sensors at the six available depths and (–0.05, –0.10, –0.30, –0.60, – 1.05 and –1.30 m) and those computed from θ_{grav}. On 40 occasions during a 34-hour long period three whole plants were sampled from the vegetation (i.e., 120 plants were sampled in total from the cover). Each plant's tiller and leaves were pooled into two separate vials. Dead material as well as the oldest living leaf around each tiller were removed in order not to contaminate tiller samples with transpiring material [Durand et al., 2007]. In addition, air water vapor was collected from the ambient atmosphere surrounding the rhizotron. The air was run at a flow rate of 1.5 l min^{-1} through two glass cold traps in series immersed in a mixture of dry ice and pure ethanol at - 80°C. Water from plant (i.e., tillers and leaves) and soil samples was extracted by vacuum distillation for 14 to 16 hours depending on the sample mass (e.g., ranging between 18 to 28 g for soil) at temperatures of 60 and 90°C, respectively. The residual water vapor pressure at the end of each successful extraction procedure invariably reached 10^{-1} mbar. The oxygen isotopic compositions of tiller, leaf, and soil water (i.e., δ_{tiller}, δ_{leaf}, and δ_{soil}) together with that of atmospheric water vapor (δ_{atm}) were measured with an IRMS (Isoprep 18 - Optima, Fison, Great-Britain, precision accuracy of 0.15 ‰). Finally, leaf water potential (ψ_{leaf}, in MPa) was monitored with a pressure chamber on two leaves per sampled plant, and evapotranspiration rate (in m d^{-1}) was derived from the changes in mass of the rhizotron at the same temporal scale as plant sampling.

Root biomass was determined from the horizontal sampling of soil between the polycarbonate sides using a 2 cm diameter auger at –0.02, –0.08, –0.10, –0.40, –0.55, –0.70, –0.90, –1.10, and –1.30 m soil depth. Each depth was sampled once to thrice. Each soil core was washed of soil particles and roots were collected over a 0.2 mm mesh filter, and dried at 60°C for 48 hours. Finally, Root Length Density (RLD, in m root (m soil)$^{-3}$) distribution was determined from the root dry mass using the specific root length determined by Gonzalez-Dugo et al. [2005] specifically for tall fescue (95 m g^{-1}). The reader is referred to Appendix C for an overview of the type and timing of the different destructive measurements during the intensive sampling period.

2.4 Modeling of RWU and δ_{tiller}

The experimental setup included about 300 tall fescue plants. In order to limit the computational requirement in the inverse modelling loop, we only generated 60 virtual root systems whose rooting depths ranged from –1.30 to –1.60 m depth [based on our own observations and those of the literature, e.g., Schulze et al., 1996; Fan et al., 2016] with the root architecture simulator CRootBox [Schnepf et al., 2018], so that the simulated RLD matched observations (Fig. 1a). In order to reach a total number of virtual plants representative of the number of plants in the experimental setup, each root system was replicated 5 times, forming a "group". Each group was assumed to occupy one sixtieth of the total horizontal area, and considered as a "big root" hydraulic network (5 identical plants per "big root") with equivalent radial and axial hydraulic conductances (thus neglecting architectural aspects but accounting for each group's respective root length density profile).

The radial soil-root conductance between the bulk soil and each group's (*i*) root surfaces in soil layer *j* ($K_{radial,j}$, m^3 MPa^{-1} d^{-1}), as derived by Meunier et al. [2017a], was assumed as variable in time (*t*):

$$K_{radial,i,j}(t) = \frac{2\pi r_{root} \cdot l_{root,i,j} \cdot B_j \cdot L_{pr} \cdot k_{soil,j}(t)}{B_j \cdot k_{soil,j}(t) + r_{root} \cdot L_{pr}} \quad (1)$$

with r_{root} (m) the root radius, $l_{root,i,j}$ (m) the root length of plants of group *i* in soil layer *j*, L_{pr} (m MPa^{-1} d^{-1}) the root radial hydraulic conductivity, $k_{soil,j}$ (m^2 MPa^{-1} d^{-1}) the soil hydraulic conductivity in layer *j*, and B_j (dimensionless) a geometrical factor simplifying the horizontal dimensions into radial domains between the bulk soil and root surfaces, as given by Schroeder et al. [2009]:

$$B_j = \frac{2(1-\rho_j)(1+\rho_j)}{2\rho_j{}^2 ln\rho_j - \rho_j{}^2 + 1} \quad (2)$$

where ρ (dimensionless) represents the ratio of the distance between roots and the root averaged diameter. It can be deduced from the observed root length density (RLD_j, m m^{-3}):

$$\rho_j = \frac{\sqrt{\frac{1}{\pi RLD_j}}}{r_{root}} \quad (3)$$

The soil hydraulic conductivity function of Mualem [1976] and van Genuchten [1980] was used:

$$k_{soil,j}(t) = k_{sat} \cdot {S_{e,j}}^{\lambda}(t) \left(1 - \left(1 - {S_{e,j}}^{\frac{1}{m}}\right)^m\right)^2 \quad (4)$$

where k_{sat} (m^2 MPa^{-1} d^{-1}), m (dimensionless) and λ (dimensionless) are soil hydraulic parameters (with m = 1 – 2/n) and $S_{e,j}$, the relative water content (dimensionless), is computed from the saturated (θ_{sat}, m^3 m^{-3}) and residual (θ_{res}, m^3 m^{-3}) water contents as:

$$S_{e,j} = \frac{\theta_j - \theta_{res}}{\theta_{sat} - \theta_{res}} \quad (5)$$

Unlike the geometrical parameter B, which defines a domain geometry between the bulk soil and roots of the overall population, the l_{root} term is group specific (*i*) and uses the simulated root length density profiles over an area corresponding to one sixtieth of the total setup horizontal area:

$$l_{root,i,j} = \frac{\Delta Z_j \cdot A_{soil} \cdot RLD_{i,j}}{60} \quad (6)$$

with ΔZ (m) and A_{soil} (m^2) the soil layer thickness and horizontal surface area, respectively.

To finalize the connection between root xylem and shoot, axial conductances per root system group (K_{axial}, m^3 MPa^{-1} d^{-1}) were calculated as equivalent "big root" specific axial conductance per root system group (k_{axial}, m^4 MPa^{-1} d^{-1}, to be optimized by inverse modelling) as:

$$K_{axial,j} = \frac{k_{axial}}{\Delta Z_j} \quad (7)$$

At each time step, both the total soil-root system conductance ($K_{soil\text{-}root}$, $m^3\ MPa^{-1}\ d^{-1}$) and the standard sink distribution (*SSF*, dimensionless, summing up to 1), were calculated from K_{radial} and K_{axial}, using the algorithm of Meunier et al. [2017b]. The variable *SSF* is the relative distribution of water uptake in each soil layer under vertically homogeneous soil water potential conditions [Couvreur et al., 2012], and $K_{soil\text{-}root}$ represents the water flow per unit water potential difference between the *SSF*-averaged bulk soil water potential and the "big leaf" (assuming a negligible stem hydraulic resistance [Steudle and Peterson, 1998]).

Adding soil hydraulic conductance to the one-dimensional hydraulic model of Couvreur et al. [2014] yields the following solutions of leaf water potential (ψ_{leaf}, MPa) and water sink terms (S, d^{-1}) whose formulation approaches that of Nimah and Hanks [1973]:

$$\psi_{leaf}(t) = -\frac{T(t)}{K_{soil-root}(t)} + \sum SSF_j(t) \cdot \psi_{soil,j}(t) \quad (8)$$

Where one sixtieth of the overall transpiration rate (T, m d^{-1}) is allocated to each group, and $\psi_{soil,j}$ (Mpa) is the soil water potential in soil layer j.

$$S_{i,j}(t) = \frac{K_{soil-root,i}(t) \cdot SSF_{i,j}(t) \cdot (\psi_{soil,j}(t) - \psi_{leaf,i}(t))}{A_{soil} \cdot \Delta Z_j} \quad (9)$$

where $K_{soil-root}$ was assumed to control the compensatory RWU which arise from a heterogeneously distributed soil water potential, due to large axial conductances [Couvreur et al., 2012].

Finally, the tiller water oxygen isotopic composition (δ_{tiller}) was calculated as the average of local soil water oxygen isotopic compositions (δ_{soil}) weighted by the relative distribution of positive water uptakes (i.e., not accounting for δ_{soil} at locations where water is exuded by the root), assuming a perfect mixture of water inside the root system [Meunier et al., 2017a]:

$$\delta_{tiller} = \frac{\sum_{S_j>0} S_j \cdot A_{soil} \cdot \Delta Z_j \cdot \delta_{soil}(t)}{\sum_{S_j>0} S_j(t) \cdot A_{soil} \cdot \Delta Z_j} \quad (10)$$

Like in the experiment, δ_{tiller} from three plants were randomly pooled at each observation time. A hundred pools of 3 plants (possibly including several plants of the same group) were randomly selected in order to obtain the pooled simulated δ_{tiller} by arithmetic averaging.

The unknown parameters of the soil-root hydraulic model, i.e., the root radial conductivity (L_{pr}), the root axial conductance (k_{axial}), the soil saturated hydraulic conductivity (k_{sat}), and the soil tortuosity factor (λ) were finally determined by inverse modeling. For details on the procedure, the reader is referred to Appendix D.

In order to evaluate the robustness of the hydraulic model predictions (parametrized solely based on the reproduction of shoot observations in the inverse modeling scheme) from independent perspectives, we also compared predictions and measurements over 4 quantitative "soil-root domain" criteria: (i) the depth at which the transition between nighttime water uptake and exudation ($S_{i,j}<0$, i.e. release of water from root to soil) takes place, (ii) quantities of exuded

water and overnight increase of soil water content, (iii) the enrichment of labelled water at the depth where water content increase is observed overnight, and (iv) the order of magnitude of the optimal root radial conductivity value as compared to literature data in tall fescue.

Finally, and as a comparison point, the Bayesian inference statistical model SIAR [Parnell et al., 2013] was used to determine the profiles of water sink terms of ten identified potential water sources. These water sources were defined to originate from 10 distinct soil layers (0.00-0.03, 0.03-0.07, 0.07-0.15, 0.15-0.30, 0.30-0.60, 0.60-0.90, 0.90-1.20, 1.20-1.32, 1.32-1.37, and 1.37-1.44 m) for which corresponding δ_{soil} values were computed [Rothfuss and Javaux, 2017]. SIAR solely bases its estimates from the comparison of δ_{tiller} observations to the isotopic compositions of the soil water sources (δ_{soil}). For this, δ_{tiller} measurements were pooled in twelve groups corresponding to different time periods, selected to best reflect the observed temporal dynamics of δ_{tiller}. The reader is here referred to Appendix E for details on the model parametrization and running procedure.

3 Results and discussion

3.1 Experimental data

3.1.1 Soil profiles

Figure 2a and b show a very stable soil water content profile and a more variable δ_{soil} profile from DaS 166 - 15:45 to DaS 168 - 05:00. Soil was dry at the surface (0.058 $m^3\ m^{-3} < \theta <$ 0.092 $m^3\ m^{-3}$ for layer 0.015 - 0.040 m) whereas closer to saturation at depth –1.30 m (θ = 0.34 $m^3\ m^{-3}$ ± 0.012 $m^3\ m^{-3}$, estimated θ_{sat} = 0.40 $m^3\ m^{-3}$, see Appendix A). According to the measured soil matric potentials (Fig. 2c), soil water was virtually unavailable (≤ –1.5 MPa) above –0.5 m depth. Soil moisture remained unchanged in the top 25 cm during the sampling period (θ = 0.08 ±0.00 $m^3\ m^{-3}$) as well as at –1.30 m from DaS 166 - 15:45 to DaS 168 - 05:00 (θ = 0.33 ±0.01 $m^3\ m^{-3}$), showing that roots were predominantly extracting water from deep soil layers.

Water in the top soil layers (–0.040 m < z < –0.015 m) was isotopically enriched (–3.2 ‰ < δ_{soil} < 0.3 ‰) as opposed to the deepest layer (δ_{soil} = –7.34 ‰ ± 0.30 ‰ at –1.30 m). Following labeling of the reservoir water on DaS 166 - 17:00, δ_{soil} reached a value of 36.9 ‰ at –1.50 m on DaS 167 - 17:00. The development of the vegetation on DaS 166-168 (LAI = 5.6) and the observed surface θ values lead us to assume that the rhizotron water losses were due to transpiration flux solely (i.e., evapotranspiration = transpiration). The soil water oxygen isotopic exponential-shaped profiles were the product of fractionating evaporation flux, and to a great extent when the soil was bare or when the tall fescue cover was not fully developed. The differences in soil water oxygen isotopic profile observed at the four different sampling dates were therefore either due to lateral heterogeneity (e.g., upper soil layers), to the soil capillary rise of labelled water from the reservoir (deep soil layers), or to the hydraulic redistribution of water through roots (to the condition that the isotopic composition of the redistributed water differs from that of the soil water at the release

location). We noted an isotopic enrichment of 1.0 ‰ of soil water observed on DaS 168 - 05:00 at –0.9 m with respect to the mean δ_{soil} value across previous sampling dates. This could partly be due to, e.g., upward preferential flow of labelled water from the bottom soil layers and therefore be the sign of the lateral heterogeneity of the soil. Another reason for this would be hydraulic redistribution of labelled water by the roots. It was however not possible to evaluate the relative importance of these three processes (lateral heterogeneity, capillary rise/preferential flow, and hydraulic redistribution) in the setting of the soil water isotopic profile since the physically-based soil-root model presented in section 2.4 does not account for soil liquid and vapor flow. This was also not the primary intent of the present study. The observed RLD profile (Fig. 1a) showed a typical exponential shape, i.e., maximum at the surface (5.42 ± 0.34 cm cm^{-3}) down to a minimum at –1.10 m (0.540 ± 0.35 cm cm^{-3}), while it increased again from the latter depth up to a value of 1.660 cm cm^{-3} at –1.30 m. This significant trend was most probably a direct consequence of the high soil water content value in this deeper layer.

3.1.2 Plant water and isotopic temporal dynamics

The temporal variation of δ_{tiller} (Fig. 3a) was found to be either (i) moderate during day and night, i.e., from DaS 167 - 06:00 to 11:00 (δ_{tiller} = –2.6 ± 1.4 ‰) and from DaS 167 - 21:30 to DaS 168 - 00:00 (δ_{tiller} = –2.7 ± 0.4 ‰), or (ii) strong during the day, i.e., from DaS 167 - 11:00 to 18:00 (maximum value of 20.9 ‰ at DaS 167 - 12:40), or else (iii) strong during the night, i.e., from DaS 167 - 04:00 to 06:00 (max = 36.4 ‰ at DaS 167 - 05:15) and from DaS 168 - 00:00 to 06:00 (max = 14.6 ‰ at 28:00, DaS 168). Note that transpiration (Fig. 3b) occurred also at night during the sampling period, due to relatively high temperature in the glasshouse leading to a value of atmospheric relative humidity smaller than 85%, Fig. 3b). From 12:00 to 14:00 and from 16:00 to 17:00 on DaS 167 (case (ii)) high values of leaf transpiration corresponded to high values of δ_{tiller}.

3.1.3 Partial decorrelation between water and isotopic state variables

Figure 4 shows that variables describing plant water status, i.e., *T* and RH (Fig. 4a) and *T* and ψ_{leaf} (Fig. 4b) were well correlated: coefficient of determination R^2 was equal to 0.78 and 0.70 for the entire experimental duration, respectively. However, linear relationships between water status and isotopic variables were either nonexistent, e.g., between *T* and δ_{tiller} (R^2=0.01, Fig. 4c) and between ψ_{leaf} and δ_{tiller} (R^2=0.00, Fig. 4h) or characterized by a low R^2 and high p-value (e.g., between *T* and δ_{leaf}, R^2=0.43, p>0.05, Fig. 4d). The partial temporal disconnection between δ_{leaf} and *T* could not be attributed to problems of the isotopic methodology, during e.g., the vacuum distillation of the water from the plant tillers and leaves: water recovery rate was always greater than 99 % and Rayleigh distillation corrections [Dansgaard, 1964; Galewsky et al., 2016] were applied to standardize the observed oxygen isotopic composition values to a 100 % water recovery (based on the comparison of sample weight loss during distillation and mass of collected distilled water). The evolution of δ_{leaf} was strongly correlated with that of δ_{tiller} during the day (R^2 = 0.90) whereas non-correlated

during the night (R^2 = 0.00, Fig. 4j). These observed correlations are in agreement with the Craig and Gordon [1965] model revisited by Dongmann [1974] and later by Farquhar et al. [2007; 2005]. The model, which is extensively used in the current literature [e.g., Dubbert et al., 2017] states that, at isotopic steady-state, δ_{leaf} is a function of the input water oxygen isotopic composition (δ_{tiller}) among other variables, i.e., leaf temperature (not measured during the experiment), stomatal and boundary layer conductances, oxygen isotopic composition of atmospheric water vapor, and relative humidity.

It is generally difficult to observe a statistically significant δ_{leaf}-δ_{tiller} (Fig. 4j) relationship at this temporal scale under natural abundance conditions in the field since the soil water isotopic weak gradient translates into weaker δ_{tiller} temporal dynamics. The quality of linear fit between δ_{leaf} and δ_{tiller} data collected during the day (R^2=0.90) was made possible in this specific experiment by the artificial isotopic labeling pulse that enhanced the soil water isotopic gradient, which in turn increased the range of variation of δ_{tiller}, ultimately highlighting the δ_{leaf}-δ_{tiller} temporal correlation. Air relative humidity is a driving variable of δ_{leaf} in the model of Dongmann [1974] via the competing terms (1–RH)·δ_{tiller} and RH·δ_{atm}, where δ_{atm} is the atmospheric water vapor isotopic composition inside the glasshouse. An overall significant linear correlation was observed between RH and δ_{leaf} during the experiment (R^2=0.57, Fig. 4g). During the two night periods (i.e., from 04:00-06:00 and from 20:30-07:00), as relative humidity increased in the glasshouse (51 % < RH < 85 %, Fig. 3b), the influence of the isotopic labeling of the tiller water (due to the labeling of deep soil water) through term (1–RH)·δ_{tiller} decreased to the benefit of term RH·δ_{atm} (with δ_{atm} values ranging from –15.9 to –10.7 ‰, mean = –13.1±1.6‰, data not shown). This was especially visible between 04:50 and 06:00 on DaS 167 and between 01:00 to 06:00 on DaS 168, when δ_{tiller} reached greater values than δ_{leaf}.

From a different perspective, as three plant water samples were pooled to reach a workable volume for the isotopic analysis at each observation time without replicates, the isotopic signal fluctuations may reflect both its temporal dynamics and its variability within the plant population.

3.2 Simulations

3.2.1 Rooting depth and transpiration rate control δ_{tiller} and ψ_{leaf} fluctuations, respectively

Despite the use of a global optimizer and 4 degrees of freedom (L_{pr}, k_{axial}, k_{sat}, λ, see optimal values in Table 1) specifically aiming at matching the simulated and observed temporal dynamics of δ_{tiller}, none of the 60 root system groups or average population could reproduce the measured fluctuations in time (R^2=0.00, Fig. 5a), regardless of the weight attributed to this criterion in the objective function. The predicted versus observed δ_{tiller} distributions including all plant groups and observation times differed noticeably but not significantly (6.6 ± 8.4 ‰ and 3.7 ± 8.4 ‰, respectively) when pooling 3 simulated δ_{tiller} randomly at each observation time (P>0.01 in 92 cases out of 100 repeated drawings), as in measurements. Besides, the simulated ψ_{leaf} fitted well the observations (R^2=0.67, overall distributions: –0.175 ± 0.053 MPa and –0.177 ± 0.053 MPa, respectively, Fig. 5c). When analyzing the distributions of ψ_{leaf} and δ_{tiller}

per maximum root system depth (Fig. 5b and d), it appears that the ψ_{leaf} signal is not sensitive to the rooting depth (Fig. 5d), while δ_{tiller} is more sensitive to rooting depth than to the temporal evolution of the plant environment (Fig. 5b). This leaves us with two hypotheses. The "rollercoaster hypothesis": δ_{tiller} rapidly goes up and down with all individuals on board of the same car (i.e. little variability within the population, unlike predictions in Fig. 5a, but like the simulated ψ_{leaf} in Fig. 5c). If that is correct, the physical model lacks a process that would capture the observed temporal fluctuations of δ_{tiller}. The "swarm pattern hypothesis": δ_{tiller} is rather stable in time but its values within the plant population are dispersed like in a flying swarm, so that δ_{tiller} values sampled at different times fluctuate, not due to temporal dynamics but to the fact that different individuals are sampled (Fig. 5a).

The model suggests that the tall fescue population ψ_{leaf} follows a "rollercoaster" dynamics driven by transpiration rate, while the population δ_{tiller} follows a "swarm" pattern driven by the maximum rooting depth of the sampled plants. As no correlation could be expected between the drivers (the maximum rooting depth of the sample plants and canopy transpiration rate), our analysis explains the absence of correlation between δ_{tiller} and ψ_{leaf} or transpiration rate.

In future experiments and in the specific context of labeling pulses, sampling more plants at each observation time would help disentangle the spatial from temporal sources of variability of ψ_{leaf} and δ_{tiller}. It would however be at the cost of the temporal resolution of observations, or would necessitate a larger setup with more plants in the case of controlled conditions experiments.

3.2.2 Independent observations support the validity of the hydraulic model predictions

In the last 12 hours of the experiment (DaS 167 – 17:00 to DaS 168 – 05:00), the measured soil water content increased by 0.029 $m^3\ m^{-3}$ at –0.9 m depth, which could be a sign of nighttime hydraulic redistribution. During the same period, the physical model predicted a cumulative water exudation sufficient to increase soil water content by 0.003 $m^3\ m^{-3}$, as soil water potential was sufficiently low to generate reverse flow, but high enough not to disrupt the hydraulic continuity between soil and roots [Carminati and Vetterlein, 2013; Meunier et al., 2017a]. While this increase is smaller than the observed water content change, it is only a component in the soil water mass balance. Given the soil water potential vertical gradient, upward soil capillary water flow may have accounted for another part of the observed moisture change. Experimental observations also show that δ_{soil} increased by 1.0 ‰ at 0.9 m depth during that time (–6.2 ‰, a value significantly higher than –7.1 ‰ ± 0.1 ‰ at earlier times based on ANOVA analysis, $P<0.01$), while our simulations of hydraulic redistribution generated an increase of δ_{soil} by 0.34 ‰. As soil capillary flow may not generate local maxima of δ_{soil} (no enrichment observed at surrounding depths, see Fig. 2b), and soil evaporation is assumed negligible at that depth, it is likely that the observed local enrichment was entirely due to hydraulic redistribution, which would then be underestimated by a factor of about 3 in our simulations. Increasing water exudation by a factor 3 would imply a simulated water content change due to exudation of 0.0090 $m^3\ m^{-3}$ absolute water content, which remains compatible with the experimental observation. Between –1.1 m and –0.9 depths, the

nighttime water flow pattern transitioned from exudation to uptake in both measurements and predictions. At –1.1 m, the model predicted a cumulative water uptake sufficient to decrease soil water content by 0.0101 $m^3\ m^{-3}$, as compared to the observed 0.0141 $m^3\ m^{-3}$ total soil water content decrease. The remaining 0.004 $m^3\ m^{-3}$ water content decrease may have contributed to the recharge to the soil layers above through capillary flow, which was not simulated. Therefore, all relevant measurements (local increase of soil water content, local enrichment of water isotopic composition) and simulation results (S<0, i.e. local water release from roots) clearly converge to the conclusion that hydraulic lift occurred in the vicinity of -0.9 m depth in the early morning of DaS 168.

As far as fitted parameter values are concerned, L_{pr} (2.3 10^{-7} m $MPa^{-1}\ s^{-1}$) was in the range found by Martre et al. [2001] in tall fescue (2.2 10^{-7} ± 0.1 m $MPa^{-1}\ s^{-1}$) and falls in the range obtained by Meunier et al. [2017a] for another grass (*Lolium multiflorum* Lam., 6.8 10^{-8} to 6.8 10^{-7} m $MPa^{-1}\ s^{-1}$). Our k_{axial} value cannot be compared to values of axial root conductance from the literature as it transfers the water absorbed by roots in a single "big root" per group of 5 identical plants. The optimal value of k_{sat} was quite high (Table 1) but reportedly very correlated to λ (i.e. soil unsaturated hydraulic conductivity is proportional to k_{sat}, but also to S_e^{λ} [van Genuchten, 1980]), so that the low value of the latter compensated the high value of the former, thus they should be considered as effective rather than physical parameters.

3.2.3 Other sources of variability and observational error

Our treatment of the soil medium in this experiment (sieving, irrigation from the bottom) makes it laterally more homogeneous than natural soils. This method allowed us to study specifically the impact of the vertical gradients of δ_{soil} on δ_{tiller}. It also justified the use of a simplistic 1-D model adapted to the vertically resolved measurements. If lateral heterogeneity of soil water content remained and was accounted for, our predictions of root water uptake distribution, δ_{tiller} and ψ_{leaf} would be altered. Observational errors in the gravimetric soil water content measurement (turned into soil water potential using the soil water retention curve) would as well alter these predictions. In order to quantify the sensitivity of our simulated results to such heterogeneity or observational error, we varied the soil water content input by ± 0.02 $m^3\ m^{-3}$ at three critical depths (–0.9, –1.1 and –1.3 m, before interpolation), at the last observation time, during which measurements and simulations suggested that hydraulic lift occurred. Our results were mostly sensitive to soil water content alterations at –0.9 m, and barely differed in response to alterations at –1.1 and –1.3 m, though the conclusions were not affected qualitatively. No statistically significant difference between predicted and observed δ_{tiller} distributions for the overall dataset could be found when pooling 3 simulated δ_{tiller} randomly at each observation time (predicted and observed δ_{tiller} distributions were closest to differ when soil water content was reduced by 0.02 $m^3\ m^{-3}$ at 0.9 m depth; P>0.01 in 76 cases out of 100 repeated drawings). Measured and simulated ψ_{leaf} remained very correlated in all cases (from R^2=0.69 to 0.74 when adding or removing 0.02 $m^3\ m^{-3}$ at 0.9 m depth, respectively). Furthermore, when adding or removing 0.02 $m^3\ m^{-3}$ at 0.9 m depth, cumulative water exudation at –0.9 m varied

between 0.0019 and 0.0035 $m^3\ m^{-3}$, uptake at –1.1 m varied between 0.0080 and 0.0108 $m^3\ m^{-3}$, and the simulated change of δ_{soil} ranged between 0.28 and 0.40 ‰, respectively.

Lateral heterogeneity of soil water isotopic composition may as well occur at the microscopic scale. As water in micropores is less mobile than water in meso- and macropores [Alletto et al., 2006], it is likely that, in the lower half of the profile, the capillary rise of labelled water affected the composition of water in meso- and macropores more than in micropores. If roots have more access to meso- and macropore water, then the water absorbed by roots would be isotopically enriched, as compared to the "bulk soil water" characterized experimentally. The importance of this possible bias depends on soil texture and heterogeneity (e.g. existence of more isolated "pockets" of soil or compact clusters), as well as on the speed of water mixing between mobile and immobile water fractions [Gazis and Feng, 2004]. Including this process in the modelling would necessitate sufficient observations to estimate the aforementioned properties, and ideally some quantification of the lateral heterogeneity of soil water isotopic composition at the micro-scale.

The lateral heterogeneity of soil hydraulic properties and root distribution may also have participated to the generation of lateral soil water potential heterogeneities, particularly in undisturbed soils. If one had access to data on lateral heterogeneity of soil properties and rooting density, it would be possible to simulate 3D soil-root water flow with a tool such as R-SWMS [Javaux et al., 2008], using a randomization technique for soil properties distribution as in Kuhlmann et al. [2012], in order to obtain estimations of the relative importance of this type of heterogeneity on δ_{tiller} and ψ_{leaf} variability.

Unlike the tiller water isotopic composition, leaf water potential turned out to be very sensitive to transpiration rate in our simulations (see temporal fluctuations of grey lines in Figure 5 panel c) and not very sensitive to root distribution (see small variations of leaf water potential across individuals in Figure 5 panel d). This suggests that in this setup the hydraulic conductance of the soil-root system limited shoot water supply more than the distribution of roots, as in Sulis et al. [2019]. Simulated baseline (i.e. for uniform transpiration rates) leaf water potentials are shown as grey lines in Figure 5 panel c, and measured leaf water potentials as a green line in the same panel. The fact that they match well, despite the high sensitivity of leaf water potential to transpiration rate, reinforces the idea that transpiration rate was likely not spatially heterogeneous among the plant population. Therefore, the tiller water isotopic composition, whose sensitivity to transpiration rate is already very low, was likely not affected by transpiration rate heterogeneity.

3.2.4 Do root water uptake profiles predicted by hydraulic and Bayesian models differ?

The root water uptake dynamics predicted by the mechanistic model are shown in Fig. 6a. The overall pattern of peaking water uptake in the lower part of the profile during daytime matched that of the statistical model, and the correlation coefficient of both model predictions was relatively high (R^2=0.53) in average over the simulation period, see Figure 7). The main differences were the following: (i) in the upper soil layers where the soil water potential was

lower –1.5 MPa, the statistical model predicted water uptake, which is theoretically impossible given the leaf water potential above –0.4 MPa [van Den Honert, 1948]; (ii) In the upper half of the profile, the physical model predicted exudation at a rate limited by the low hydraulic conductivity between root surface and bulk soil, with a peak at night, at –0.9 m depth (quantitative analysis in previous section); (iii) Below –1.0 m depth, the water uptake rate predicted by the statistical model steadily increased with depth while that of the physical model was more uniform, likely due to axial hydraulic limitation [e.g., Bouda et al., 2018] counteracting the increasing soil water potential with depth. Note that the outcome of the statistical model may significantly depend on the definition of the a priori relative RWU (rRWU) profile. In the present study, we set it to follow a "flat" uniform distribution (i.e., $rRWU_j = 1/10$, see Appendix E), in other words, each layer was initially defined to contribute equally to RWU. To the contrary of other studies [e.g., Mahindawansha et al., 2018], where the a priori rRWU profile was empirically constructed on basis of soil water content and root length density profiles, we decided not to further arbitrarily constrain the Bayesian model for the sake of comparison with the physically-based soil-root model.

3.3 Progresses and Challenges in soil water isotopic labeling for RWU determination

Often in the field, the vertical dynamics of both soil water oxygen and hydrogen isotopic compositions are not strong enough (or show convolutions leading to issues of identifiability) for partitioning RWU among different contributing soil water sources. As a consequence, we unfortunately cannot make use of the natural variability in isotopic abundances for deciphering soil-root transfer processes [Beyer et al., 2018; Burgess et al., 2000]. To address this limitation of the isotopic methodology, labeling pulses have been applied locally at different depths in the soil profile [e.g., Beyer et al., 2016] or at the soil upper/lower boundaries under both lab and field conditions by mimicking rain events [e.g., Piayda et al., 2017] and/or rise of the groundwater table [Meunier et al., 2017a; Kühnhammer et al., 2019]. After labeling, we are faced with two problems: (i) the labeling pulse might enhance RWU at the labeling location if the volume of added water significantly changes the value of soil water content. It therefore poses the question of the meaningfulness of the derived RWU profiles, and this independently from the model used (i.e., physically-based soil-root model or statistical multi-source mixing model). In other worlds: are we observing a natural RWU behavior of the plant individual or population or are we seeing the influence of the labeling pulse? Certainly a way to move forward is environmental observatories such as ecotron and field lysimeters [e.g., Groh et al., 2018; Benettin et al., 2018] that provide means to better constrain hydraulic boundary conditions and reduced their isotopic heterogeneity. They allow for a mechanistic and holistic understanding of soil-root processes from stable isotopic analysis.

Another topic of concern is (ii) the difficulty to properly observe in situ (1) the propagation of the labeling pulse in the soil after application and (2) the temporal dynamics of the plant RWU isotopic composition. Beyer and Dubbert [2019] presented a comprehensive review on recent isotopic techniques for non-destructive, online, and continuous determination of soil and plant water isotopic compositions [e.g., Rothfuss et al., 2013; Quade et al., 2019; Volkmann

et al., 2016a] as alternatives of the widely used combination of destructive sampling and offline isotopic analysis following cryogenic vacuum extraction [Orlowski et al., 2016b] or liquid-vapor direct equilibration [Wassenaar et al., 2008]. These techniques have the potential for a paradigm change in isotopic studies on RWU processes to the condition that, e.g., isotopic effects during sample collection are fully understood.

The present study highlights the need not to "trust" our isotope data alone and always complement them by information on environmental factors as well as on soil and plant water status to go beyond the simple application of statistical models. This is especially the case in the framework of labeling studies where strong soil water isotopic gradients may induce strong dynamics of the RWU isotopic composition from a low variability of rooting depths.

4 Conclusion

In the present study, light could be shed on RWU of *Festuca arundinacae* by specifically manipulating the lower boundary conditions for water content and oxygen isotopic composition. The new version of the one-dimensional model of Couvreur et al. (2014) implemented here accounted for both root and soil hydraulics in a population of "big" root systems of known root length density profile. This approach underlined the high sensitivity of δ_{tiller} to rooting depth and suggested that if δ_{tiller} is measured on a limited number of individuals, its variations in time may reflect the heterogeneity of rooting depth within the population, rather than temporal dynamics which was minor in our simulations. The model avoided the prediction of water uptake at locations where it was physically unavailable (e.g., in the top half of the soil profile), by accounting for water potential differences observed between the leaves and the soil, and explained quantitatively the local isotopic enrichment of soil water as the occurrence of nighttime Hydraulic Lift at –0.9 m depth. On the other hand, the Bayesian statistical approach tested for comparison, which was driven by isotopic information solely, naturally translated the observed changes of δ_{tiller} into profound temporal dynamics of RWU, at the expense of eco-physiological consideration (e. g., temporal dynamics of leaf water potential and transpiration rate).

This case study highlights (i) the potential limitations of water isotopic labeling techniques for studying RWU: the soil water isotopic artificial gradients induced from water addition result in an improvement in RWU profiles determination to the condition that they are properly characterized spatially and temporally. As already pointed out in the review of Rothfuss and Javaux (2017), the study also (ii) underlines the interest of complementing in-situ isotopic observations in soil and plant water with information on soil water status and plant ecophysiology; it finally (iii) calls for the use of simple soil-root models (though requiring additional water status measurements and making more explicit assumptions on the description of the soil-plant system, as compared to the traditional Bayesian approach) for inversing isotopic data and gain insights into the RWU process.

Acknowledgements

The experiment was part of the ASCHYD ("Biogeochemical characterization of Hydraulic Lift") project and supported by the French EC2CO/BIOHEFFECT program (CNRS – INSU, ANDRA, BRGM, CNES, IFREMER, IRSTEA, IRD, INRA and Météo France). During the preparation of this manuscript, V.C. was supported by the Belgian National Fund for Scientific Research (FNRS, FC 84104) the Interuniversity Attraction Poles Programme-Belgian Science Policy (grant IAP7/29), and the "Communauté française de Belgique-Actions de Recherches Concertées" (grant ARC16/21-075); FM was first funded by the BAEF and the WBI,then by the FWO as a junior postdoc and is thankful to these organizations for their support.

Data sets

Upon acceptance, all research data needed for creating plots will be available in reliable FAIR-aligned data repositories with assigned DOIs.

Author contribution

TB, JLD, and PB designed the experiments and TB, JLD, PB, and YR carried them out. VC, FM, and MJ developed the physically-based root water uptake model code and VC and FM performed the simulations. YR performed the statistical simulations. VC, YR, FM, and MJ prepared the manuscript with contributions from all co-authors.

Competing interests

The authors declare that they have no conflict of interest.

References

Alletto, L., Coquet, Y., Vachier, P., and Labat, C. (2006), Hydraulic Conductivity, Immobile Water Content, and Exchange Coefficient in Three Soil Profiles, Soil Science Society of America Journal, 70, 1272-1280, 10.2136/sssaj2005.0291.

Benettin, P., Volkmann, T. H. M., von Freyberg, J., Frentress, J., Penna, D., Dawson, T. E., and Kirchner, J. (2018), Effects of climatic seasonality on the isotopic composition of evaporating soil waters, Hydrol. Earth Syst. Sc., 22, 2881-2890, 10.5194/hess-22-2881-2018.

Beyer, M., Koeniger, P., Gaj, M., Hamutoko, J. T., Wanke, H., and Himmelsbach, T. (2016), A deuterium-based labeling technique for the investigation of rooting depths, water uptake dynamics and unsaturated zone water transport in semiarid environments, J. Hydrol., 533, 627-643, 10.1016/j.jhydrol.2015.12.037.

Beyer, M., Hamutoko, J. T., Wanke, H., Gaj, M., and Koeniger, P. (2018), Examination of deep root water uptake using anomalies of soil water stable isotopes, depth-controlled isotopic labeling and mixing models, J. Hydrol., 566, 122-136, 10.1016/j.jhydrol.2018.08.060.

Beyer, M., and Dubbert, M. (2019), X Water Worlds and how to investigate them: A review and future perspective on in situ measurements of water stable isotopes in soils and plants, Hydrol. Earth Syst. Sci. Discuss., in review 10.5194/hess-2019-600.

Bouda, M., Brodersen, C., and Saiers, J. (2018), Whole root system water conductance responds to both axial and radial traits and network topology over natural range of trait variation, J. Theor. Biol., 456, 49-61, 10.1016/j.jtbi.2018.07.033.

Burgess, S. S. O., Adams, M. A., Turner, N. C., and Ward, B. (2000), Characterisation of hydrogen isotope profiles in an agroforestry system: implications for tracing water sources of trees, Agric. Water Manage., 45, 229-241, Doi 10.1016/S0378-3774(00)00105-0.

Carminati, A., and Vetterlein, D. (2013), Plasticity of rhizosphere hydraulic properties as a key for efficient utilization of scarce resources, Ann. Bot., 112, 277-290, 10.1093/aob/mcs262.

Couvreur, V., Vanderborght, J., and Javaux, M. (2012), A simple three-dimensional macroscopic root water uptake model based on the hydraulic architecture approach, Hydrol. Earth Syst. Sc., 16, 2957-2971, 10.5194/hess-16-2957-2012.

Couvreur, V., Vanderborght, J., Beff, L., and Javaux, M. (2014), Horizontal soil water potential heterogeneity: simplifying approaches for crop water dynamics models, Hydrol. Earth Syst. Sc., 18, 1723-1743, 10.5194/hess-18-1723-2014.

Craig, H., and Gordon, L. I.: Deuterium and oxygen 18 variations in the ocean and marine atmosphere, Stable Isotopes in Oceanographic Studies and Paleotemperatures, Spoleto, Italy, 1965, 9-130, 1965.

Dansgaard, W. (1964), Stable Isotopes in Precipitation, Tellus, 16, 436-468, 10.1111/j.2153-3490.1964.tb00181.x.

Dongmann, G. (1974), Contribution of Land Photosynthesis to Stationary Enrichment of O-18 in Atmosphere, Radiat. Environ. Biophys., 11, 219-225, 10.1007/Bf01323191.

Dubbert, M., Kübert, A., and Werner, C. (2017), Impact of Leaf Traits on Temporal Dynamics of Transpired Oxygen Isotope Signatures and Its Impact on Atmospheric Vapor, Fontiers in Plant Science, 8, 5, 10.3389/fpls.2017.00005.

Dubbert, M., and Werner, C. (2019), Water fluxes mediated by vegetation: emerging isotopic insights at the soil and atmosphere interfaces, New Phytol., 221, 1754–1763, 10.1111/nph.15547.

Durand, J. L., Bariac, T., Ghesquière, M., Biron, P., Richard, P., Humphreys, M., and Zwierzykovski, Z. (2007), Ranking of the depth of water extraction by individual grass plants using natural 18O isotope abondance, Environ. Exp. Bot, 60, 137-144.

Fan, J. L., McConkey, B., Wang, H., and Janzen, H. (2016), Root distribution by depth for temperate agricultural crops, Field Crops Res., 189, 68-74, 10.1016/j.fcr.2016.02.013.

Farquhar, G. D., and Cernusak, L. A. (2005), On the isotopic composition of leaf water in the non-steady state, Funct. Plant Biol., 32, 293-303, 10.1071/Fp04232.

570 Farquhar, G. D., Cernusak, L. A., and Barnes, B. (2007), Heavy water fractionation during transpiration, Plant Physiol.,
571 143, 11-18, 10.1104/pp.106.093278.
572 Galewsky, J., Steen-Larsen, H. C., Field, R. D., Worden, J., Risi, C., and Schneider, M. (2016), Stable isotopes in
573 atmospheric water vapor and applications to the hydrologic cycle, Rev. Geophys., 54, 809-865,
574 10.1002/2015rg000512.
575 Gazis, C., and Feng, X. (2004), A stable isotope study of soil water: evidence for mixing and preferential flow paths,
576 Geoderma, 119, 97-111, https://doi.org/10.1016/S0016-7061(03)00243-X.
577 Gonfiantini, R. (1978), Standards for stable isotope measurements in natural compounds, Nature, 271, 534-536,
578 10.1038/271534a0.
579 Gonzalez-Dugo, V., Durand, J. L., Gastal, F., and Picon-Cochard, C. (2005), Short-term response of the nitrogen
580 nutrition status of tall fescue and Italian ryegrass swards under water deficit, Aust. J. Agric. Res., 56, 1269-
581 1276, 10.1071/Ar05064.
582 Groh, J., Stumpp, C., Lucke, A., Putz, T., Vanderborght, J., and Vereecken, H. (2018), Inverse Estimation of Soil
583 Hydraulic and Transport Parameters of Layered Soils from Water Stable Isotope and Lysimeter Data, Vadose
584 Zone J., 17, UNSP 170168
585 10.2136/vzj2017.09.0168.
586 Grossiord, C., Gessler, A., Granier, A., Berger, S., Brechet, C., Hentschel, R., Hommel, R., Scherer-Lorenzen, M., and
587 Bonal, D. (2014), Impact of interspecific interactions on the soil water uptake depth in a young temperate
588 mixed species plantation, J. Hydrol., 519, 3511-3519, 10.1016/j.jhydrol.2014.11.011.
589 Javaux, M., Schroder, T., Vanderborght, J., and Vereecken, H. (2008), Use of a three-dimensional detailed modeling
590 approach for predicting root water uptake, Vadose Zone J., 7, 1079-1088.
591 Jesch, A., Barry, K. E., Ravenek, J. M., Bachmann, D., Strecker, T., Weigelt, A., Buchmann, N., de Kroon, H., Gessler,
592 A., Mommer, L., Roscher, C., and Scherer-Lorenzen, M. (2018), Belowground resource partitioning alone
593 cannot explain the biodiversity–ecosystem function relationship: A field test using multiple tracers, J. Ecol.,
594 106, 2002–2018., 10.1111/1365-2745.12947.
595 Kuhlmann, A., Neuweiler, I., van der Zee, S. E. A. T. M., and Helmig, R. (2012), Influence of soil structure and root
596 water uptake strategy on unsaturated flow in heterogeneous media, Water Resour. Res., 48,
597 10.1029/2011wr010651.
598 Kühnhammer, K., Kübert, A., Brüggemann, N., Deseano Diaz, P., van Dusschoten, D., Javaux, M., Merz, S.,
599 Vereecken, H., Dubbert, M., and Rothfuss, Y. (2019), Investigating the root plasticity response of Centaurea
600 jacea to soil water availability changes from isotopic analysis, New Phytol., 226, 98-110, 10.1111/nph.16352
601 Mahindawansha, A., Orlowski, N., Kraft, P., Rothfuss, Y., Racela, H., and Breuer, L. (2018), Quantification of plant
602 water uptake by water stable isotopes in rice paddy systems, Plant Soil, 10.1007/s11104-018-3693-7.
603 Martre, P., Cochard, H., and Durand, J.-L. (2001), Hydraulic architecture and water flow in growing grass tillers
604 (Festuca arundinacea Schreb.), Plant Cell Environ, 24, 65-76, 10.1046/j.1365-3040.2001.00657.x.
605 Meunier, F., Rothfuss, Y., Bariac, T., Biron, P., Durand, J.-L., Richard, P., Couvreur, V., J, V., and Javaux, M. (2017a),
606 Measuring and modeling Hydraulic Lift of *Lolium multiflorum* using stable water isotopes, Vadose Zone J.,
607 10.2136/vzj2016.12.0134.
608 Meunier, F., Couvreur, V., Draye, X., Vanderborght, J., and Javaux, M. (2017b), Towards quantitative root hydraulic
609 phenotyping: novel mathematical functions to calculate plant-scale hydraulic parameters from root system
610 functional and structural traits, J. Math. Biol., 75, 1133-1170, 10.1007/s00285-017-1111-z.
611 Meunier, F., Draye, X., Vanderborght, J., Javaux, M., and Couvreur, V. (2017c), A hybrid analytical-numerical method
612 for solving water flow equations in root hydraulic architectures, Appl. Math. Model., 52, 648-663,
613 10.1016/j.apm.2017.08.011.
614 Mualem, Y. (1976), A new model predicting the hydraulic conductivityof unsaturated porous media, Water Resour.
615 Res., 12, 513-522, 10.1029/WR012i003p00513.
616 Nimah, M. N., and Hanks, R. J. (1973), Model for Estimating Soil-Water, Plant, and Atmospheric Interrelations. 1.
617 Description and Sensitivity, Soil Sci. Soc. Am. J., 37, 522-527, 10.2136/sssaj1973.03615995003700040018x.

618 Oerter, E., and Bowen, G. (2019), Spatio-temporal heterogeneity in soil water stable isotopic composition and its
619 ecohydrologic implications in semiarid ecosystems, Hydrol. Process., 33, 1724–1738, 10.1002/hyp.13434.
620 Orlowski, N., Breuer, L., and McDonnell, J. J. (2016a), Critical issues with cryogenic extraction of soil water for stable
621 isotope analysis, Ecohydrology, 9, 3-10, 10.1002/eco.1722.
622 Orlowski, N., Pratt, D. L., and McDonnell, J. J. (2016b), Intercomparison of soil pore water extraction methods for
623 stable isotope analysis, Hydrol. Process., 30, 3434-3449, 10.1002/hyp.10870.
624 Orlowski, N., Breuer, L., Angeli, N., Boeckx, P., Brumbt, C., Cook, C. S., Dubbert, M., Dyckmans, J., Gallagher, B.,
625 Gralher, B., Herbstritt, B., Herve-Fernandez, P., Hissler, C., Koeniger, P., Legout, A., Macdonald, C. J.,
626 Oyarzun, C., Redelstein, R., Seidler, C., Siegwolf, R., Stumpp, C., Thomsen, S., Weiler, M., Werner, C., and
627 McDonnell, J. J. (2018), Inter-laboratory comparison of cryogenic water extraction systems for stable isotope
628 analysis of soil water, Hydrol. Earth Syst. Sc., 22, 3619-3637, 10.5194/hess-22-3619-2018.
629 Parnell, A. C., Phillips, D. L., Bearhop, S., Semmens, B. X., Ward, E. J., Moore, J. W., Jackson, A. L., Grey, J., Kelly,
630 D. J., and Inger, R. (2013), Bayesian stable isotope mixing models, Environmetrics, 24, 387–399,
631 10.1002/env.2221.
632 Passot, S., Couvreur, V., Meunier, F., Draye, X., Javaux, M., Leitner, D., Pages, L., Schnepf, A., Vanderborght, J., and
633 Lobet, G. (2019), Connecting the dots between computational tools to analyse soil-root water relations, J.
634 Exp. Bot., 70, 2345-2357, 10.1093/jxb/ery361.
635 Piayda, A., Dubbert, M., Siegwolf, R., Cuntz, M., and Werner, C. (2017), Quantification of dynamic soil-vegetation
636 feedbacks following an isotopically labelled precipitation pulse, Biogeosciences, 14, 2293-2306, 10.5194/bg-
637 14-2293-2017.
638 Quade, M., Klosterhalfen, A., Graf, A., Brüggemann, N., Hermes, N., Vereecken, H., and Rothfuss, Y. (2019), In-situ
639 Monitoring of Soil Water Isotopic Composition for Partitioning of Evapotranspiration During One Growing
640 Season of Sugar Beet (Beta vulgaris), Agr. Forest Meteorol., 266–267, 53–64,
641 10.1016/j.agrformet.2018.12.002.
642 Rothfuss, Y., Vereecken, H., and Brüggemann, N. (2013), Monitoring water stable isotopic composition in soils using
643 gas-permeable tubing and infrared laser absorption spectroscopy, Water Resour. Res., 49, 1-9,
644 10.1002/wrcr.20311.
645 Rothfuss, Y., and Javaux, M. (2017), Reviews and syntheses: Isotopic approaches to quantify root water uptake: a
646 review and comparison of methods, Biogeosciences, 14, 2199-2224, 10.5194/bg-14-2199-2017.
647 Schnepf, A., Leitner, D., Landl, M., Lobet, G., Mai, T. H., Morandage, S., Sheng, C., Zorner, M., Vanderborght, J.,
648 and Vereecken, H. (2018), CRootBox: a structural-functional modelling framework for root systems, Ann.
649 Bot., 121, 1033-1053, 10.1093/aob/mcx221.
650 Schroeder, T., Javaux, M., Vanderborght, J., Korfgen, B., and Vereecken, H. (2009), Implementation of a Microscopic
651 Soil-Root Hydraulic Conductivity Drop Function in a Three-Dimensional Soil-Root Architecture Water
652 Transfer Model, Vadose Zone J., 8, 783-792, 10.2136/vzj2008.0116.
653 Schulze, E. D., Mooney, H. A., Sala, O. E., Jobbagy, E., Buchmann, N., Bauer, G., Canadell, J., Jackson, R. B., Loreti,
654 J., Oesterheld, M., and Ehleringer, J. R. (1996), Rooting depth, water availability, and vegetation cover along
655 an aridity gradient in Patagonia, Oecologia, 108, 503-511, 10.1007/Bf00333727.
656 Sprenger, M., Leistert, H., Gimbel, K., and Weiler, M. (2016), Illuminating hydrological processes at the soil-
657 vegetation-atmosphere interface with water stable isotopes, Review of Geophysics, 54, 674-704,
658 10.1002/2015RG000515.
659 Steudle, E., and Peterson, C. A. (1998), How does water get through roots?, J. Exp. Bot., 49, 775-788.
660 Sulis, M., Couvreur, V., Keune, J., Cai, G. C., Trebs, I., Junk, J., Shrestha, P., Simmer, C., Kollet, S. J., Vereecken,
661 H., and Vanderborght, J. (2019), Incorporating a root water uptake model based on the hydraulic architecture
662 approach in terrestrial systems simulations, Agricultural and Forest Meteorology, 269, 28-45,
663 10.1016/j.agrformet.2019.01.034.
664 van Den Honert, T. H. (1948), Water transport in plants as a catenary process, Discuss. Faraday Soc., 3, 146-153,
665 10.1039/DF9480300146.

van Genuchten, M. T. (1980), A closed-form equation for predicting the hydraulic conductivity of unsaturated soils, Soil Sci. Soc. Am. J., 44, 892-898, 10.2136/sssaj1980.03615995004400050002x.
Volkmann, T. H., Kühnhammer, K., Herbstritt, B., Gessler, A., and Weiler, M. (2016a), A method for in situ monitoring of the isotope composition of tree xylem water using laser spectroscopy, Plant Cell Environ, 10.1111/pce.12725.
Volkmann, T. H. M., Haberer, K., Gessler, A., and Weiler, M. (2016b), High-resolution isotope measurements resolve rapid ecohydrological dynamics at the soil–plant interface, New Phytol., 10.1111/nph.13868.
Washburn, E. W., and Smith, E. R. (1934), The isotopic fractionation of water by physiological processes, Science, 79, 188-189, 10.1126/science.79.2043.188.
Wassenaar, L. I., Hendry, M. J., Chostner, V. L., and Lis, G. P. (2008), High resolution pore water delta2H and delta18O measurements by H2O(liquid)-H2O(vapor) equilibration laser spectroscopy, Environ. Sci. Technol., 42, 9262-9267.
Werner, C., Schnyder, H., Cuntz, M., Keitel, C., Zeeman, M. J., Dawson, T. E., Badeck, F. W., Brugnoli, E., Ghashghaie, J., Grams, T. E. E., Kayler, Z. E., Lakatos, M., Lee, X., Maguas, C., Ogee, J., Rascher, K. G., Siegwolf, R. T. W., Unger, S., Welker, J., Wingate, L., and Gessler, A. (2012), Progress and challenges in using stable isotopes to trace plant carbon and water relations across scales, Biogeosciences, 9, 3083-3111, 10.5194/bg-9-3083-2012.
Yakir, D., and Sternberg, L. D. L. (2000), The use of stable isotopes to study ecosystem gas exchange, Oecologia, 123, 297-311, 10.1007/s004420051016.

5 Tables

	L_{pr} (m MPa^{-1}s^{-1})	k_{axial} (m^4 MPa^{-1} s^{-1})	k_{sat} (m^2 MPa^{-1} s^{-1})	λ (-)
Lower limit	10^{-11}	10^{-13}	10^{-5}	–5
Upper limit	10^{-6}	10^{-8}	10^{-2}	2
Value at best fit	$2.3\ 10^{-7}$	$4.5\ 10^{-11}$	$9.5\ 10^{-3}$	–4.9

Table 1. Optimum and limits of the four-dimensional parametric space explored by the global optimization algorithm aiming at minimizing the difference between simulated and observed δ_{tiller} and ψ_{leaf}, as well as their standard deviation from average values during the full experiment.

6 Figures

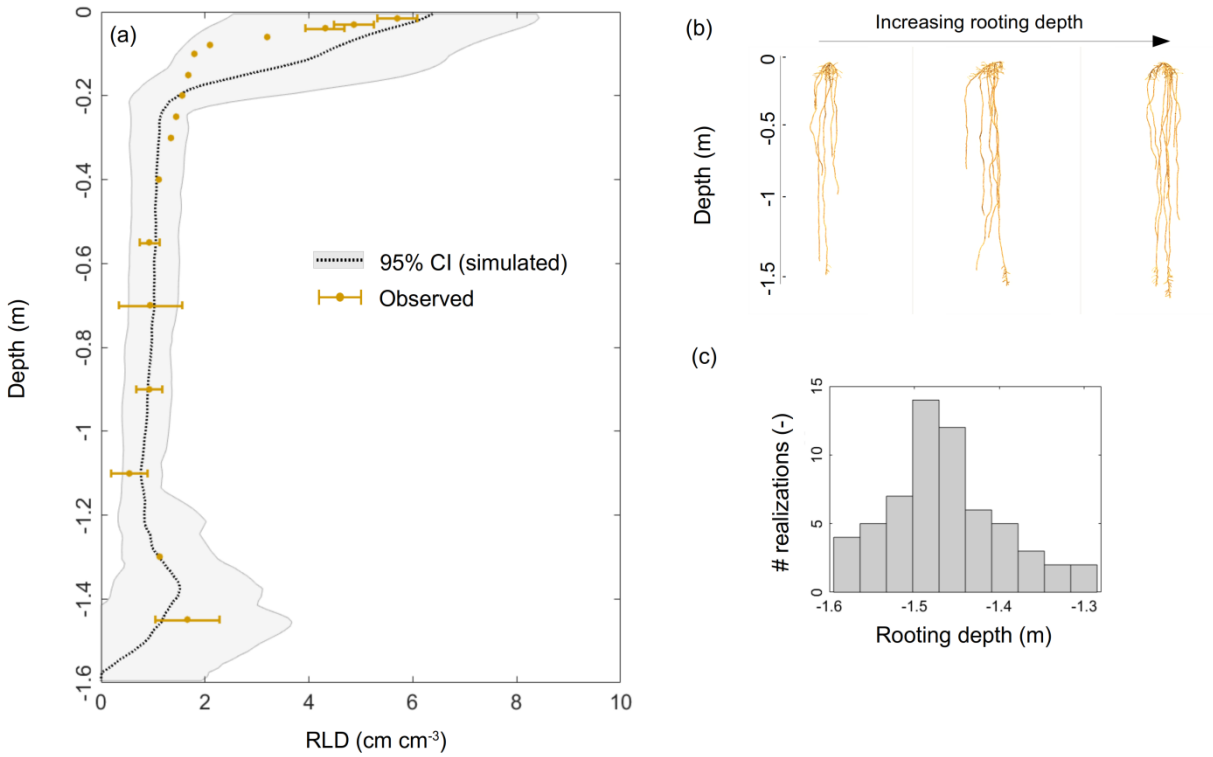

Figure 1. (a) Simulated (grey envelopes) and observed (brown dots) root length density profiles. Panels (b) and (c) illustrate the variability in modelled root system architectures and rooting depths, respectively.

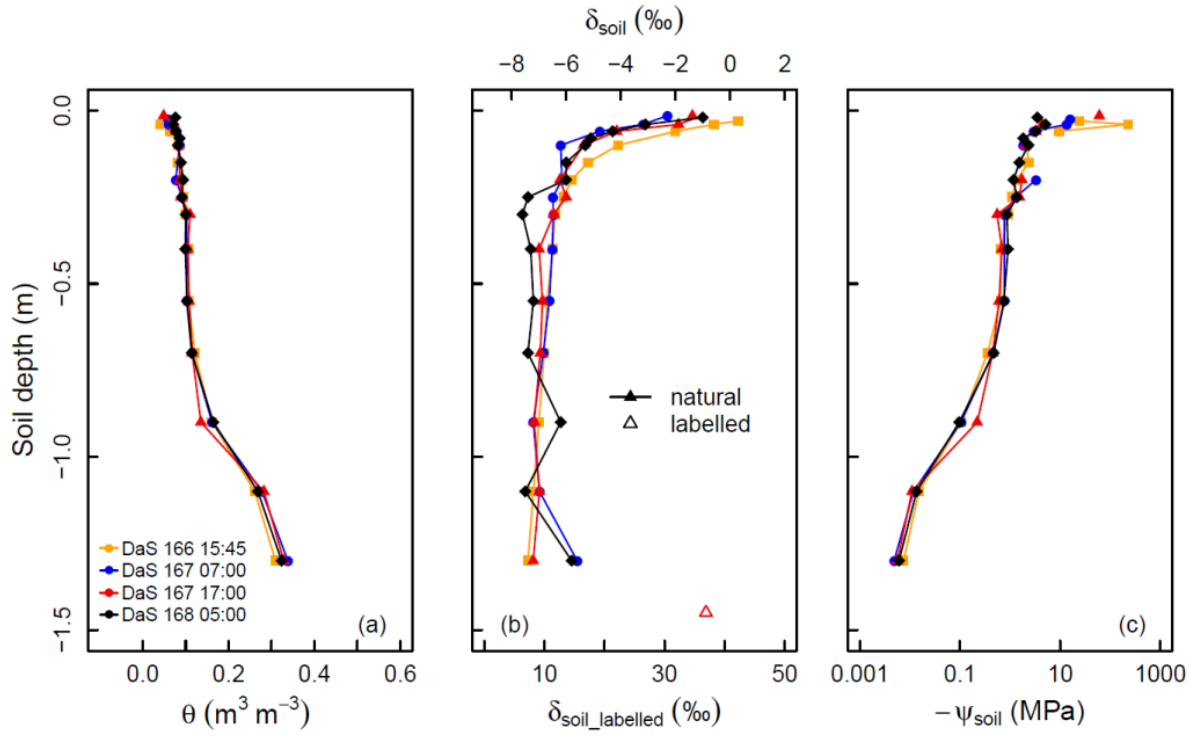

694

695 **Figure 2. Measured soil volumetric water content (θ, panel a), oxygen isotopic composition (δ_{soil}, panel b), and calculated**
696 **soil matric potential (ψ_{soil}, panel c) profiles during the sampling period.**

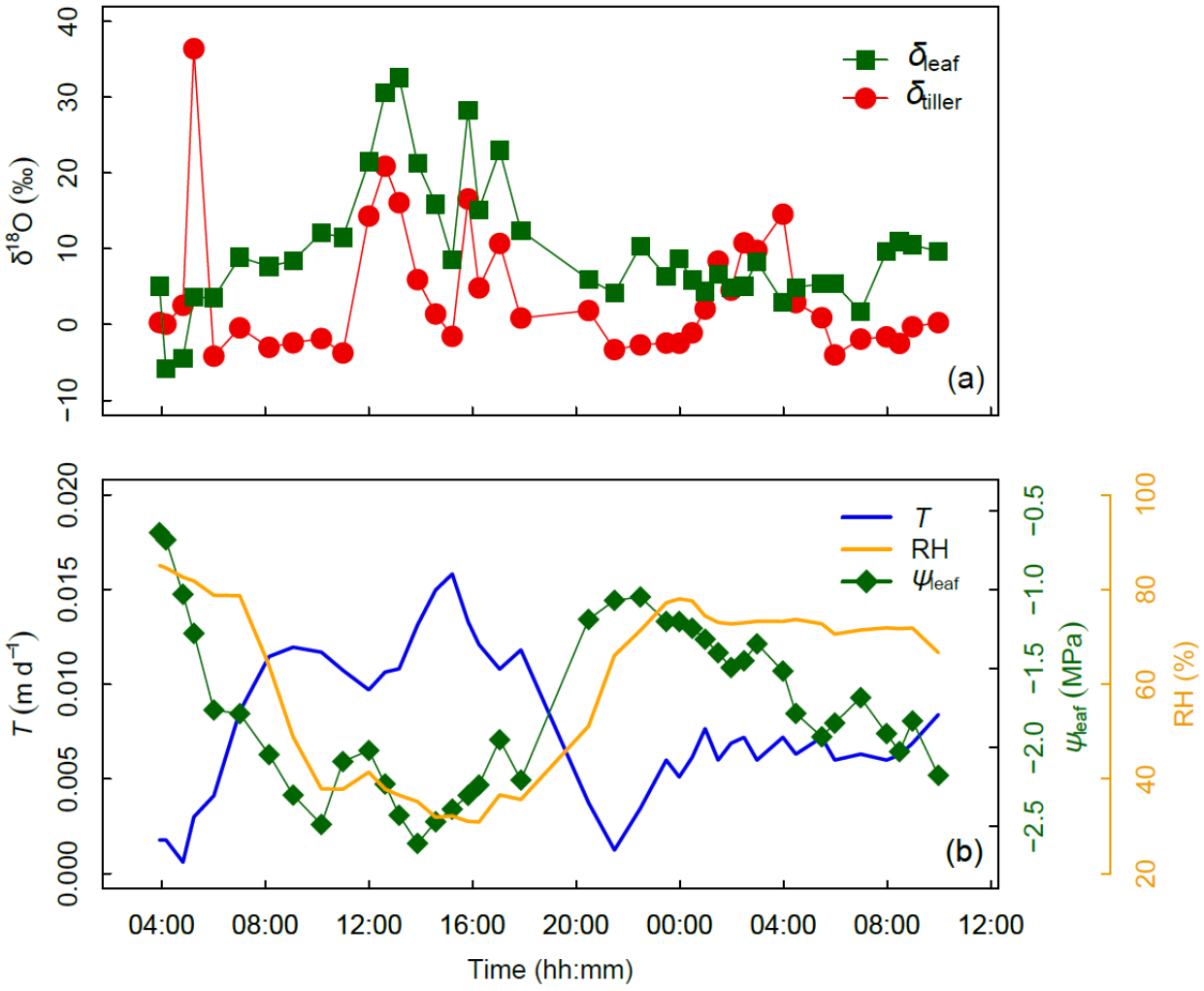

697

698 **Figure 3. (a) Time series of tiller and leaf water oxygen isotopic compositions (δ_{tiller} and δ_{soil}, ‰). (b) Transpiration flux (*T*,**
699 **in m d^{-1}), relative humidity (HR, %), and leaf water potential (ψ_{leaf}, in MPa, panel b) from days after seeding DaS 167 –**
700 **04:00 to DaS 168 – 11:00. Time of Labeling was DaS 166 – 17:00.**

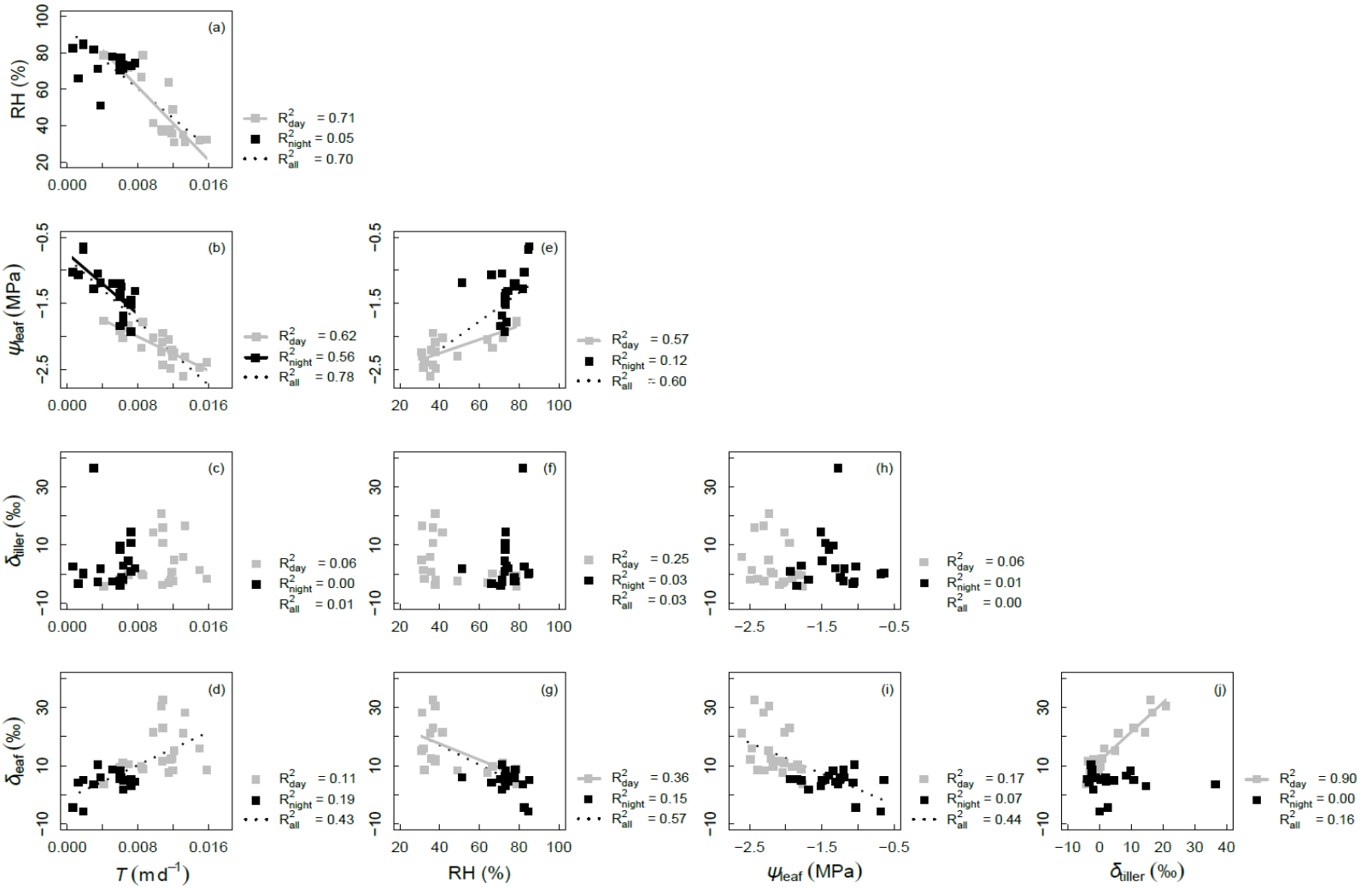

Figure 4. Correlations between measured variables: oxygen isotopic compositions of xylem and leaf waters (δ_{tiller} and δ_{leaf}, in ‰), transpiration rate (T, in m d^{-1}), relative humidity (RH, %), and leaf water potential (ψ_{leaf}, in MPa). Coefficient of determinations (R^2) are reported for all data, and separately for 'day' data (gray symbols) and 'night' data (black symbols) (see Appendix C for definition of 'day' and 'night' experimental periods). Regression lines are drawn for linear models with p-value < 0.01

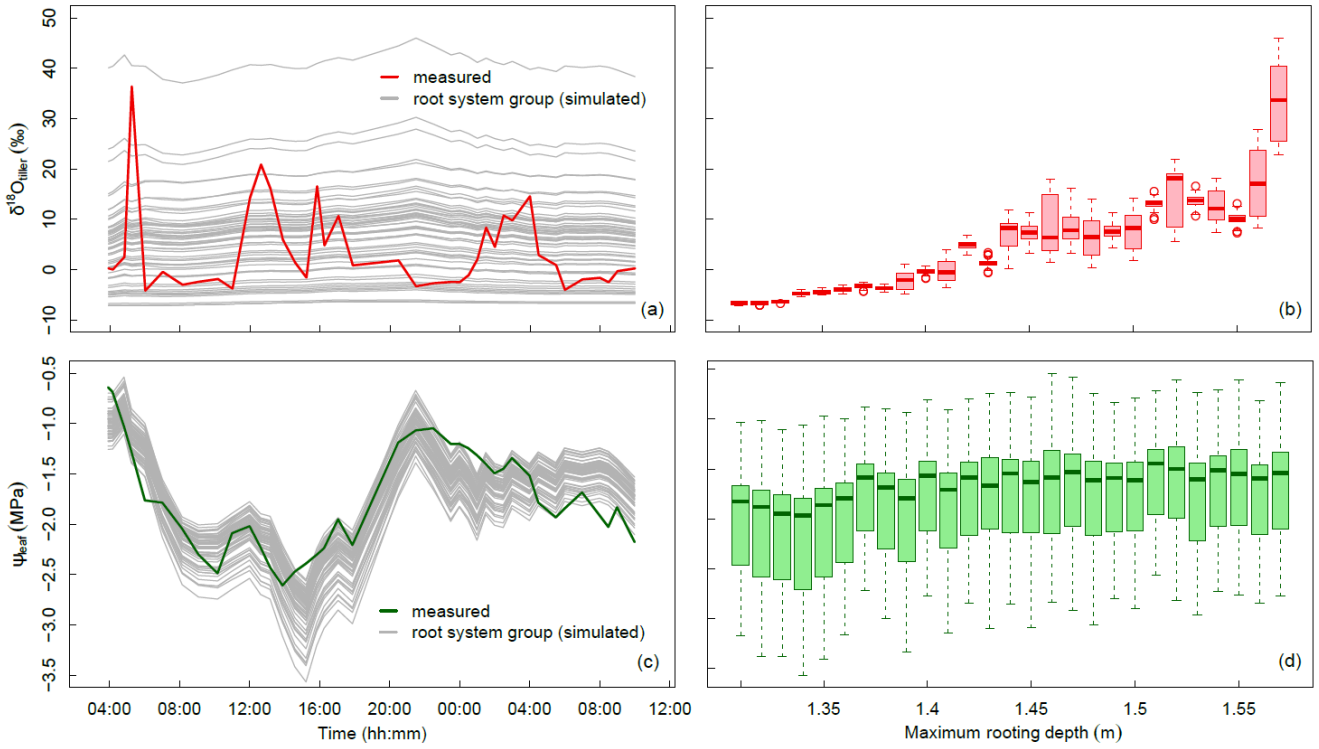

Figure 5. Variation of δ_{tiller} and ψ_{leaf} in time and across the 60 groups of simulated root systems. (a) Temporal dynamics of δ_{tiller} measured (thick red line) and simulated (thin grey lines, one line per root system group, following a "swarm" pattern). (b) Boxplot of simulated δ_{tiller} values for each root system maximum depth, by 1 cm increment. (c) Temporal dynamics of ψ_{leaf} measured (thick green line) and simulated (thin grey lines, one line per root system group, following a "rollercoaster" pattern). (d) Boxplot of simulated ψ_{leaf} values for each root system maximum depth, by 1 cm increment.

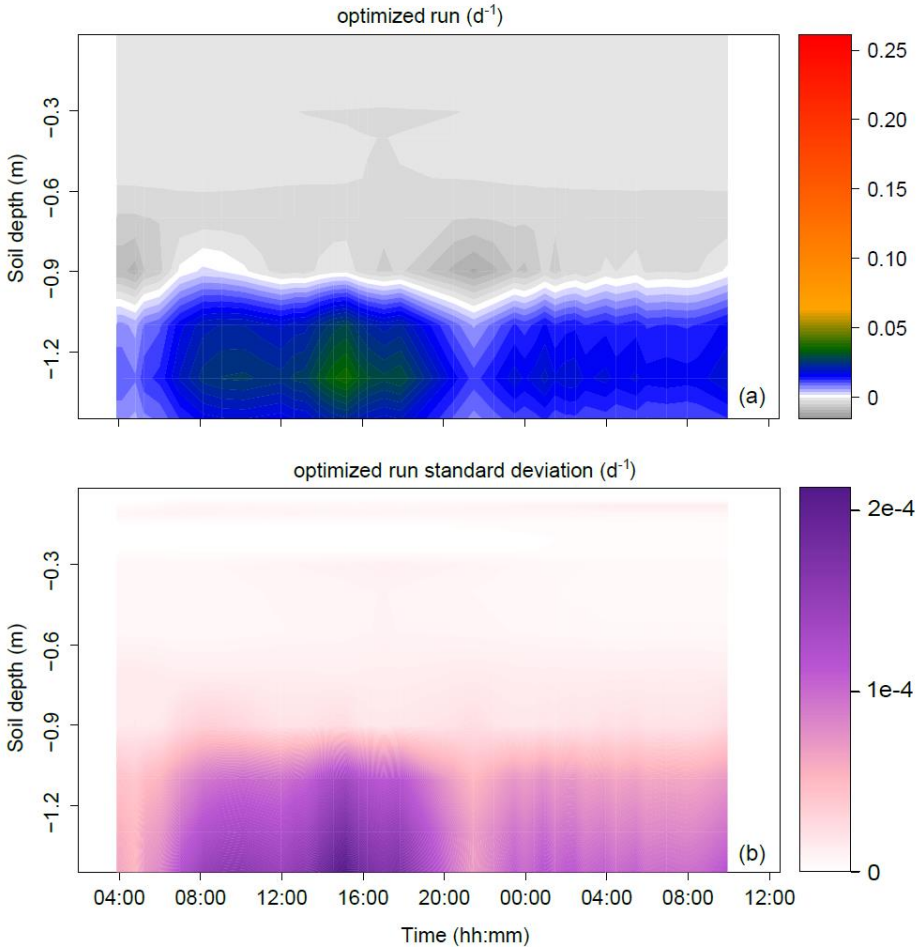

Figure 6. Time series of the profiles of root water uptake per unit soil volume (sink term, d^{-1}) computed with the physically-based model. (a) Sum of sink terms across the 60 groups of the population. (b) Variability of sink terms within the 60 groups of the population (1 standard deviation).

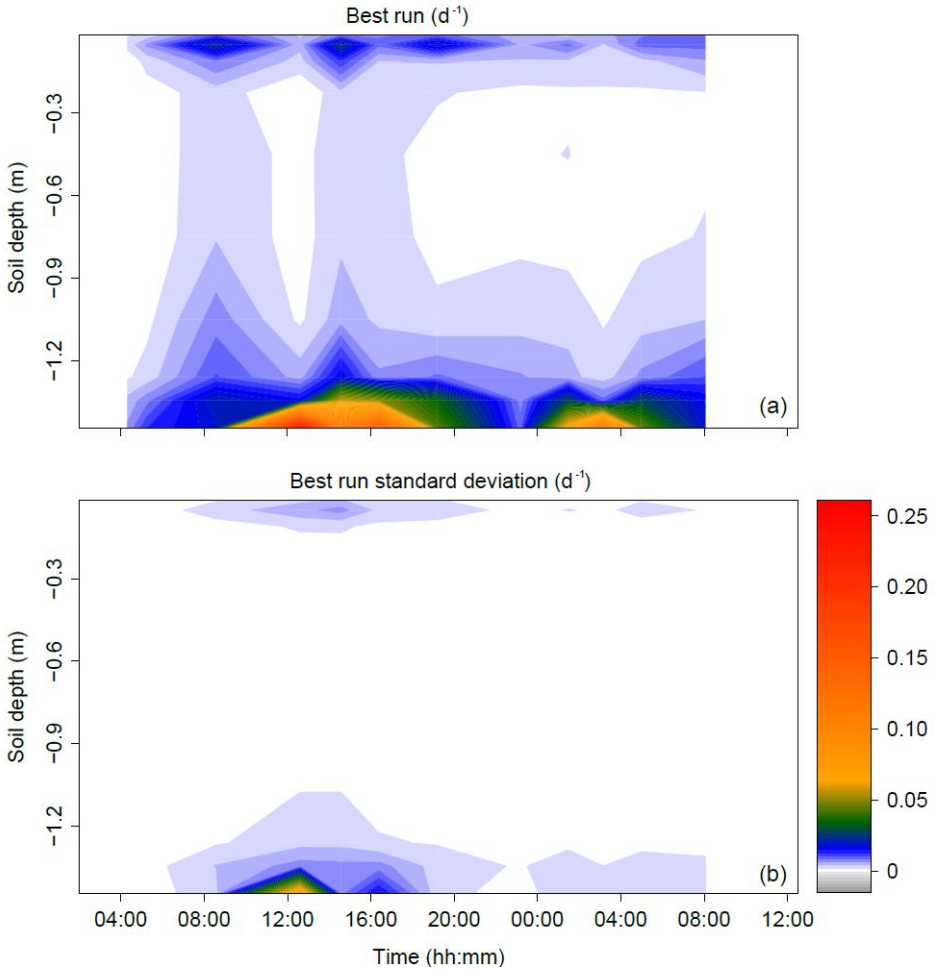

Figure 7. Time series of the profiles of root water uptake per unit soil volume (sink term, d^{-1}) computed with the statistical model SIAR (a). Panel (b) reports the variance of the estimated sink term (1 standard deviation).

7 Appendix

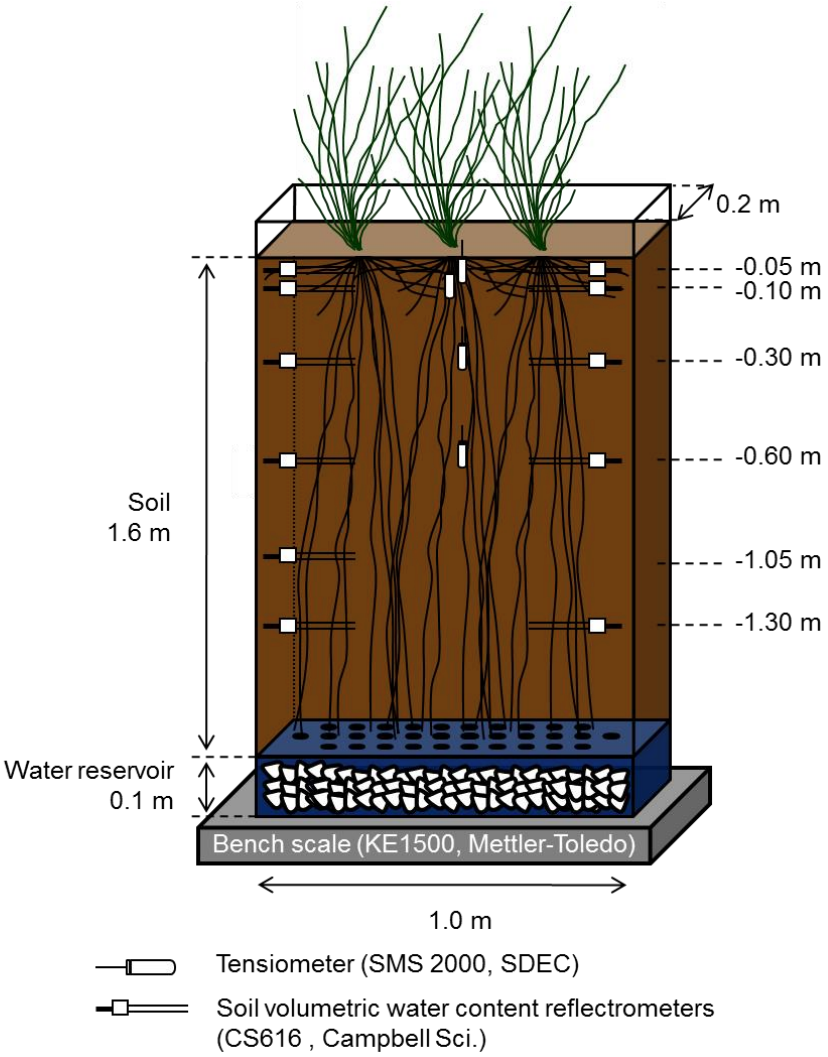

Appendix A. Soil macro-rhizotron experimental setup with tall fescue cover

θ_{sat} (m^3 m^{-3})	θ_{res} (m^3 m^{-3})	α (m^{-1})	n (-)
0.4	0.044	0.0285	2.29

Appendix B. Soil retention curve and parameters optimized values [van Genuchten, 1980 - Burdine] [Meunier et al., 2017a]

728 **Appendix C. Timeline of destructive sampling**

	DAS 166	DAS 167																						
		‘night’ data					‘day’ data															‘night data’			
Time	15:45	03:55	04:10	04:50	05:15	06:00	07:00	08:10	09:05	10:10	11:00	12:00	12:40	13:10	13:55	14:35	15:15	15:50	16:15	17:00	17:50	20:30	21:30	22:30	23:30
Soil	x						x													x					
Leaves		x	x	x	x	x	x	x	x	x	x	x	x	x	x	x	x	x	x	x	x	x	x	x	x
roots	x																								

	DAS 168																
	‘night data’												‘day’ data				
Time	00:00	00:30	01:00	01:30	02:00	02:30	03:00	04:00	04:30	05:00	05:30	06:00	07:00	08:00	08:30	09:00	10:00
Soil										x							
Leaves	x	x	x	x	x	x	x	x	x		x	x	x	x	x	x	x

729

Appendix D. Inverse modeling scheme

The parametrization method was inverse modeling, with four targets: (i) minimizing the differences between observed and predicted δ_{tiller} in each pool *p*, (ii) minimizing the difference between the standard deviations of observed and predicted δ_{tiller} (temporal and population deviations altogether), (iii) minimizing the differences between observed and predicted ψ_{leaf} in each root system group *i*, (iv) minimizing the difference between the standard deviations of observed and predicted δ_{tiller} (temporal and population deviations altogether). These targets translated as an objective function (*OF*) to be minimized, where differences were normalized by the standard deviation (*SD*) of observations in order to make the error function dimensionless:

$$OF = \sqrt{\frac{1}{2}\left(\frac{1}{N_p N_t}\sum_i \sum_t \left(\frac{\delta_{tiller,obs}(t)-\delta_{tiller,p,sim}(t)}{SD\left(\delta_{tiller,obs}(t)\right)}\right)^2 + \frac{1}{N_i N_t}\sum_i \sum_t \left(\frac{\psi_{leaf,obs}(t)-\psi_{leaf,i,sim}(t)}{SD\left(\psi_{leaf,obs}(t)\right)}\right)^2\right)} + \left|\frac{SD(\delta_{tiller,obs}(t))-SD(\delta_{tiller,p,sim}(t))}{SD(\delta_{tiller,obs}(t))}\right| + \left|\frac{SD(\psi_{leaf,obs}(t))-SD(\psi_{leaf,i,sim}(t))}{SD(\psi_{leaf,obs}(t))}\right| \quad \text{(D1)}$$

where N_p is the number of δ_{tiller} pools simulated (100) at each observation time, N_i is the number of plant groups simulated (60), and N_t the total number of observation times (40).

The global optimizer Multistart heuristic algorithm OQNLP (Optimal Methods Inc.) of the MATLAB (The MathWorks, Inc., USA) optimization toolbox was used to minimize the error function within the lower and upper limits of the parametric space reported in Table 1.

Appendix E. Statistical determination of relative RWU profiles with SIAR

The Bayesian inference statistical model SIAR [Parnell et al., 2013] was used to determine the profiles of relative contributions to RWU (rRWU, dimensionless) of ten identified potential water sources. These water sources were defined to originate from the soil layers 0.00-0.03, 0.03-0.07, 0.07-0.15, 0.15-0.30, 0.30-0.60, 0.60-0.90, 0.90-1.20, 1.20-1.32, 1.32-1.37, and 1.37-1.44 m. Their corresponding isotopic compositions were obtained from the measured soil water isotopic compositions (δ_{soil}) and volumetric content (θ) values following Eq. (E1) [Rothfuss and Javaux, 2017]:

$$\delta_{soil,J} = \frac{\sum_{j \in J} \delta_{soil,j} \cdot \theta_j \cdot \Delta Z_j}{\sum_{j \in J} \theta_j \cdot \Delta Z_j} \quad \text{(E1)}$$

where J is the soil layer index, j is the soil sub-layer index, and ΔZ_j is the thickness of the soil sub-layer j. Therefore, equation (E1) translates the soil water isotopic composition measured across sub-layers j into representative isotopic compositions of the different sources (i.e., across layers J). The computed $\delta_{soil,J}$ were compared to δ_{tiller} values. For this, δ_{tiller} measurements were pooled in twelve groups corresponding to different time periods. These groups were defined to best reflect the apparent temporal dynamics of δ_{tiller}.

For each of the twelve time periods:

(i) the function *siarmcmcdirichletv4* of the SIAR R package (https://cran.r-project.org/web/packages/siar/index.html) was run 500,000 times with prescribed burnin and thinby equal to 50000 and 15, respectively. The output of the model (i.e., the *a posteriori* rRWU distribution across the ten soil water sources J) was obtained from a flat Dirichlet *a priori* rRWU distribution (i.e., $rRWU_J$=1/10);

(ii) the 'best run' (*br*, dimensionless) was selected from SIAR's output. It was defined as the closest solution of relative contributions across sources from the set of most frequent values (*mfv*, dimensionless), i.e., the relative contribution with the greatest probability of occurrence. The best run was identified as minimizing the objective function below, i.e., the RMSE (root mean square error) with respect to the set of mfv_J:

$$OF = \sqrt{\frac{\sum_{J=1}^{10} \left(mfv_J - br_J\right)^2}{10}} \quad \text{(E2)}$$

(iii) *br* was then multiplied by transpiration rate (in m d^{-1}) and divided by soil layer thicknesses (ΔZ_J, in m) to obtain sink terms (S_J, i.e. root water uptake rate per unit soil volume, expressed in d^{-1}). The interest of sink terms in a comparison is that they do not vary with soil vertical discretization.

Steps (i)-(iii) were repeated a 1,000 times to estimate the variance of the best run for each time period and soil water source J.